J Mater Sci (2009) 44:2553–2559
DOI 10.1007/s10853-009-3333-y

Amorphous and nano crystalline phase formation in Ni_2MnGa ferromagnetic shape memory alloy synthesized by melt spinning

Raghupatruni Venkata Satya Prasad · Gandham Phanikumar

Received: 30 November 2008 / Accepted: 9 February 2009 / Published online: 6 March 2009
© Springer Science+Business Media, LLC 2009

Abstract Melt spinning technique was used to synthesize Ni_2MnGa ferromagnetic shape memory alloy ribbons. Transmission electron microscopy (TEM) and atomic force microscopy (AFM) analysis of the ribbon synthesized at lower wheel speed (20 m/s) reveal the formation of very fine clusters of austenitic phase of Ni_2MnGa. However at higher wheel speed (30 m/s) the formation of martensite and nanoparticles of Ni_2MnGa with a size range of 10–20 nm in the amorphous matrix is observed. Also an amorphous phase was observed at higher wheel speed in some areas of the ribbon. Annealing (1000 °C, 1 h) of the ribbon synthesized at higher wheel speed resulted in martensite and γ (gamma) phases. Amorphous phase, Ni_2MnGa nanoparticles, and the martensite phase are analyzed in detail.

Introduction

Rapid solidification by melt spinning is a well-studied processing technique by which one can produce a variety of materials with extraordinary properties [1]. There are numerous applications for rapidly solidified alloys by melt spinning such in electrical and magnetic appliances, ribbons for transformer cores and bearing materials [2]. In melt spinning wheel speed and thickness of the ribbon are known to be important parameters as they affect the thermal field at the solid/liquid interface strongly and result in significant interface under cooling. Melt spinning results in the microstructures with refined grain sizes, increased solubility of alloying elements, reduced levels of segregation and in some cases formation of metastable crystalline and amorphous phases [3].

Ferromagnetic shape memory alloys such as Ni_2MnGa are a new class of materials that attracted the attention of research community [4, 5]. Ferromagnetic shape memory alloys are different from conventional shape memory alloys because of their ability to exhibit the shape memory effect in the presence of magnetic field. Ni_2MnGa alloys show giant magnetic field induced strain of about 9.5% at ambient temperature, which made this material a potential candidate for the fabrication of magnetic shape memory (MSM) pumps, valves, and actuators [6]. These alloys undergoes a typical transformation sequence as follows: P → 5M → 7M → T or P → 7M → T, where P stands for the Parent Phase ($L2_1$), 5M—five layer modulated (Tetragonal), 7M—seven layer modulated (Orthorhombic), and the T non-modulated (Tetragonal) which is the most stable martensitic phase and, therefore, it exists at low temperatures [7]. These transformation sequences are highly dependent on compositional homogeneity and also for most of the actuator applications, relatively large single crystals or coarse grained, preferentially oriented polycrystalline materials are desirable. Earlier workers observed that the conventional solidification resulted in compositional inhomogeneity [8], which in turn affected the key parameters, such as the transformation strain, twinning flow stress, and magneto crystalline anisotropy in Ni_2MnGa alloys [9]. In rapidly solidified alloys, kinetics of solidification are very fast resulting in very fine length scale of segregation (about 1 μm). Chemical homogeneity is relatively easier to achieve [10]. Ni_2MnGa alloys are also known to be fragile

R. V. S. Prasad · G. Phanikumar (✉)
Department of Metallurgical and Materials Engineering, Indian Institute of Technology Madras, Chennai 600036, India
e-mail: gphani@iitm.ac.in

R. V. S. Prasad
e-mail: rvsp@smail.iitm.ac.in

and studies on imparting ductility to these alloys concentrated on processes, such as melt spinning, spark plasma sintering, and sputtering [11]. Recent investigations like twin boundary motion by ab initio methods, magneto-microstructural coupling, thermo mechanical behavior, and wear behavior of shape memory alloys kept the research on Ni–Mn–Ga alloys intense in last decade [12–15]. Efforts were mainly concentrated on the evaluation of magnetic and shape memory properties of these alloys but the studies on microstructure modifications using rapid solidification are limited.

In this work, we study the rapid solidification behavior of Ni_2MnGa alloy by melt spinning technique and highlight the phase evolution that depends on the processing conditions by presenting the microstructural characterization in detail.

Experimental

Ni_2MnGa alloy is prepared by vacuum arc melting of the 99.99% pure nickel, manganese, and gallium in an argon atmosphere. Five gram button samples were prepared and melted 4 times to ensure a highly homogeneous ingot. A conventional copper wheel was used for melt spinning ribbons of the Ni_2MnGa alloy under vacuum. Wheel speeds chosen for characterization of corresponding samples are optimized after several trails to obtain long ribbon of good quality. In each case, (for 20 and 30 m/s wheel speed) approximately 5 g of alloy was induction melted in a quartz tube having an orifice diameter of 0.8 mm, and ejected with a 1.10 bar back-pressure of argon gas. The ribbons at different wheel speeds obtained after melt spinning were characterized using transmission electron microscopy[1] and atomic force microscopy.[2] Phase identification was also confirmed using X-ray diffraction[3] studies using Cu-K_α radiation. Uniformity of the ribbons across thickness has been confirmed by SEM of the cross sections, as well as XRD patterns from both the sides of the ribbon.

Results and discussion

Melt spun alloy

Melt spun ribbon synthesized at 20 m/s is termed as MSP-1. The same ribbon after annealing at 1000 °C/1 h is termed as MSP-1 HT. Similarly the ribbon melt spun at 30 m/s is denoted as MSP-2, and the one after annealing at 1000 °C/1 h as MSP-2 HT. The notations for respective wheel speeds, heat treatment, melt spun ribbon sample dimensions, and summary of phases formed for each case are given in Table 1. The XRD patterns of the MSP-1, MSP-1 HT, MSP-2, and MSP-2 HT are shown in Fig. 1. Figures 4, 6, 7, 8 show the transmission electron microscopy results of the melt spun samples. Results from atomic force microscopy are shown in Figs. 3, 5. The observations and discussion from the characterization studies of the MSP-1, MSP-1 HT, MSP-2, and MSP-2 HT samples are as follows.

Low wheel speed ribbon (MSP-1)

Figure 1 shows X-ray diffraction (XRD) profile of the MSP-1 sample (pattern at the bottom of the figure). The pattern was indexed to the austenite phase (with $L2_1$ Heusler atomic order) of Ni_2MnGa and it can also be observed that the peaks were very sharp indicating crystalline nature of the sample. For the same ribbon (MSP-1) the TEM bright field image and corresponding selected area electron diffraction (SAED) pattern were shown in Fig. 2a, b. In the bright field image (Fig. 2a) the g-vector corresponding to [2 2 4] direction is shown and SAED pattern (Fig. 2b) was taken with the $[\bar{1}\,3\,\bar{1}]$ zone axis. From the bright field image very fine crystals over the whole area can be seen. An AFM image made on polished and electrolytically etched samples taken in contact mode is shown in Fig. 3. From Fig. 3a it can be clearly confirmed that grains were homogeneously distributed. Image analysis of grain size versus (area) percentage of grains is shown in Fig. 3b. From this analysis the average grain size reported as 80–180 nm. The formation of very fine crystals in the case of MSP-1 may be attributed due to high nucleation rate at the melt-wheel interface where the cooling rate is high. The wheel speed for this sample is lower (20 m/s) of the two reported and the corresponding under cooling would be relatively lower [16] resulting in fine crystals. Lower wheel speeds would result in lower under cooling of the melt. During solidification, due to release of latent heat, the recalescence could result in bringing the liquid to the equilibrium melting point resulting in slower kinetics of solidification. Thus, the sample contains homogenously distributed fine equiaxed crystals as opposed to amorphous phase formation [17, 18] as shown by TEM and AFM micrographs from Figs. 2 and 3, respectively.

High wheel speed ribbon (MSP-2)

From the room temperature XRD pattern of MSP-2 (as shown in Fig. 1), corresponding peaks were indexed to martensite phase of Ni_2MnGa with non-modulated

[1] Philips CM12.

[2] Dimension 3100 atomic force microscope, Nanoscope IV (Digital Instruments, USA).

[3] Bruker Discover D8 diffractometer.

Table 1 Summary of melt spun ribbon samples details

S.No	Wheel speed (m/s) and heat treatment	Sample identification	Ribbon width and thickness	Phases present
1	20	MSP-1	3 mm and 30–35 μm	Fine crystals of Ni_2MnGa (Austenite with $L2_1$ atomic ordering) (80–180 nm)
2	Annealed (20 m/s) ribbon at 1000 °C for 1 h	MSP-1 HT	3 mm and 30–35 μm	Austenite with $L2_1$ atomic ordering
3	30	MSP-2	3 mm and 20–25 μm	Martensite (with non-modulated tetragonal structure), Ni_2MnGa nanoparticles (10–20 nm) and amorphous phase
4	Annealed (30 m/s) ribbon at 1000 °C for 1 h	MSP-2 HT	3 mm and 20–25 μm	Martensite (with non-modulated tetragonal structure) and γ (gamma) phase

Austenite with $L2_1$ atomic ordering (lattice parameter $a = 0.5825$ nm)

Martensite with non-modulated tetragonal structure (lattice parameter $a = b = 0.5920$ nm, and $c = 0.5566$ nm with $c/a = 0.94$)

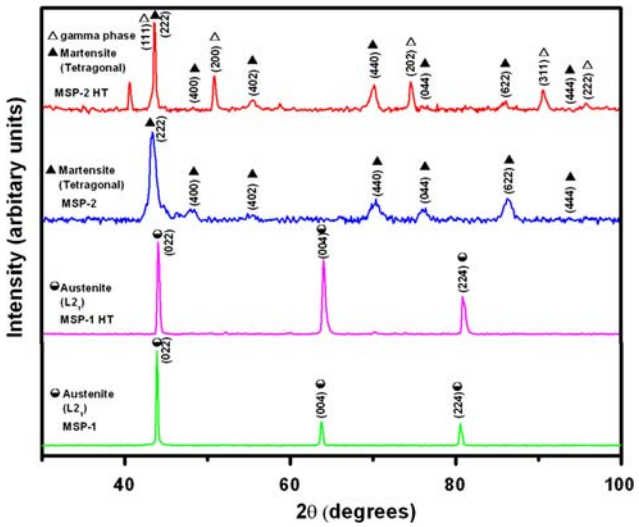

Fig. 1 XRD patterns of MSP-1, MSP-1 HT (annealed at 1000 °C/1 h), MSP-2, and MSP-2 HT (annealed at 1000 °C/1 h) samples

tetragonal structure [19]. To understand the phase transformations, extensive TEM analysis was done as shown in Fig. 4, 6, 7. Figure 4a, b shows the TEM images of MSP-2. The bright field image represented by the g-vector corresponding to $[2\,\bar{2}\,2]$ direction shows the martensite phase. The selected area electron diffraction pattern as shown in Fig. 4b taken with [4 4 0] zone axis confirms that the martensite phase belongs to non-modulated tetragonal structure. In the bright field image (Fig. 4a) martensite twins, as well as twin variants are represented by arrow marks. The selected area electron diffraction pattern (SAED) shows the streaks and it is obvious from the pattern that the mirror plane of the twinned reflections and the streaks are perpendicular to the striations in the TEM images. These reflections confirms that the striations are {2 2 2} twins and belongs to the martensite phase (non-modulated tetragonal structure) of Ni_2MnGa alloy. The angle between the basal planes of the variants A and C measured from bright field TEM image and reported as 120°–125°. The included angle between variants A and C is measured from the corresponding SAED pattern as shown in the Fig. 4b, which is around 55°–60° [20]. The Fig. 5 represents the AFM image of the MSP-2 sample. From the image one can confirm that those alternative layers are the twins of martensite. The size of twins of martensite phase is determined to be about 20–120 nm from the image analysis as shown in Fig. 5b.

Figure 6a, b, c shows the TEM images and SAED pattern of MSP-2 at different location. From the bright field image

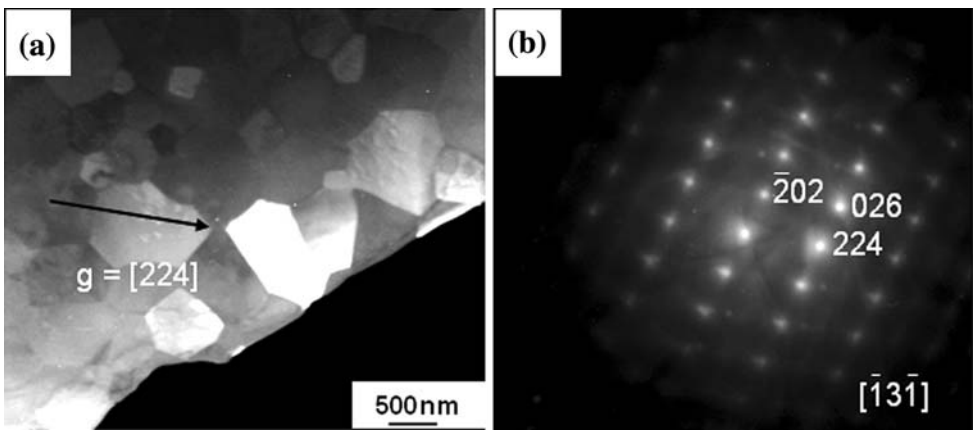

Fig. 2 TEM micrographs of **a** bright field image MSP-1 sample, **b** SAED pattern of MSP-1 sample

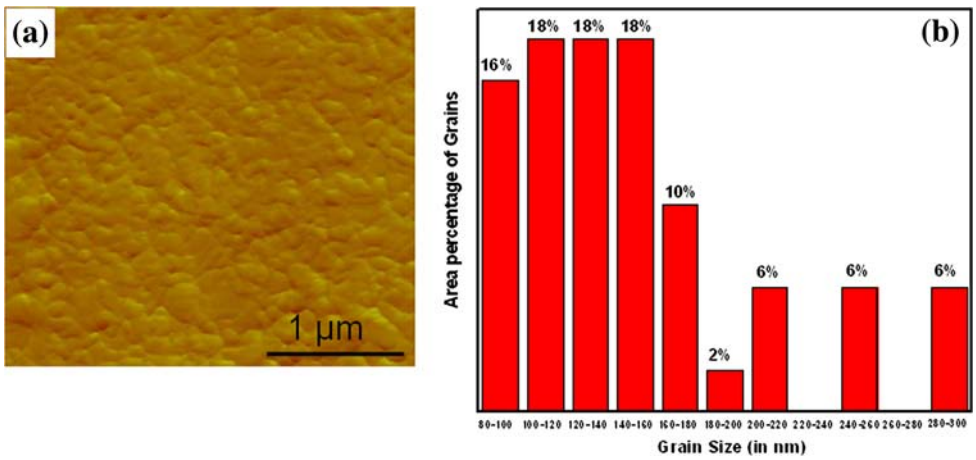

Fig. 3 **a** AFM micrograph of MSP-1 sample **b** Image analysis of MSP-1 sample

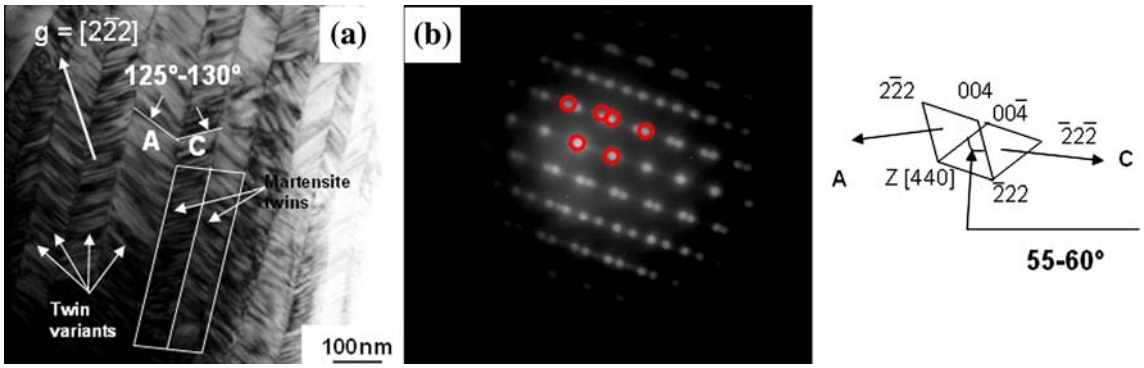

Fig. 4 TEM micrographs of **a** bright field image MSP-2 sample, **b** SAED pattern of MSP-2 sample

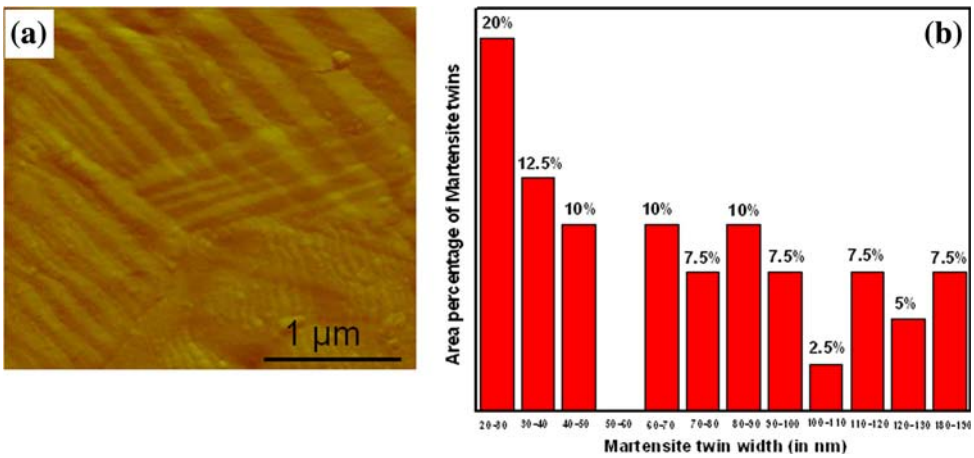

Fig. 5 **a** AFM micrograph of MSP-2 sample **b** Image analysis of MSP-2 sample

(Fig. 6a) black particles of nanometer size can be seen and the same particles appeared bright in the corresponding dark field image (Fig. 6b). The reflections from SAED pattern taken on these nanoparticles confirm that they are Ni_2MnGa particles. These nanoparticles are clearly shown by triangular markers in both the bright field and dark filed images. The size of the nano crystalline particles was calculated from the dark field image (Fig. 6b) and found to be in between 10 and 20 nm. The peak broadening in the XRD pattern of this sample could thus be attributed to these regions of fine clusters in a matrix that is likely to be amorphous. Figure 7a, b, c shows the bright field and SAED pattern of MSP-2 sample from different region. From the bright field image (Fig. 7a) the amorphous phase can be seen surrounded by martensite twins. The amorphous phase represented clearly by a circle in the bright filed image and the same phase can be seen at higher magnification in Fig. 7b. In Fig. 7c the corresponding selected area electron diffraction (SAED) pattern

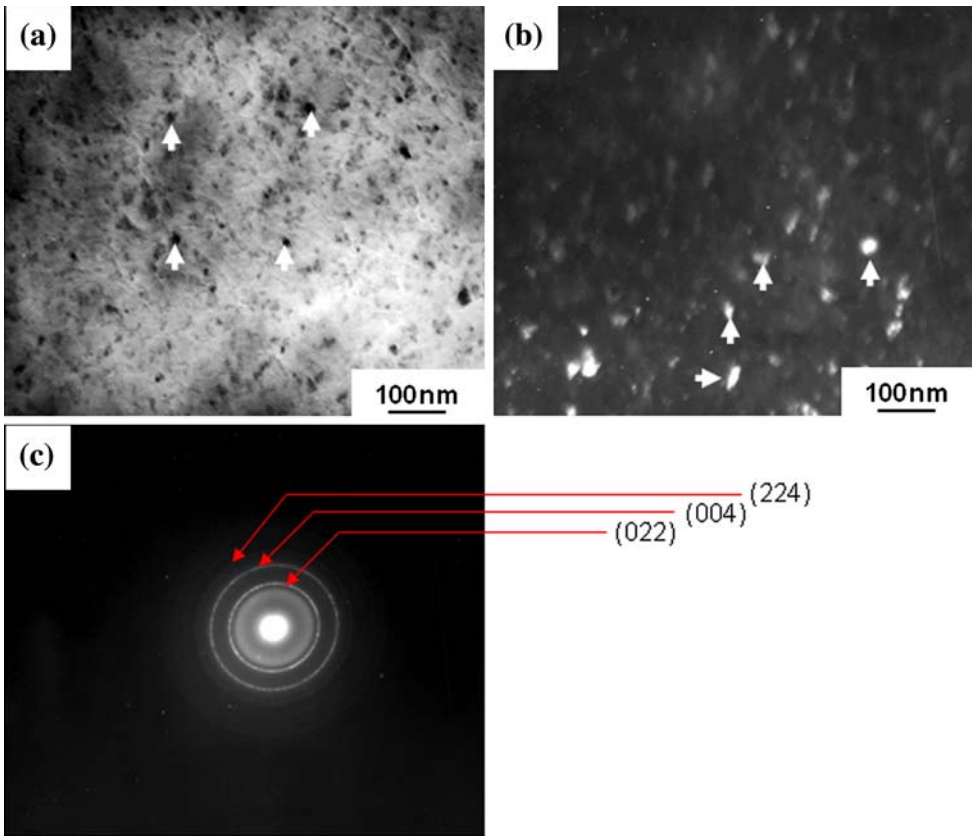

Fig. 6 TEM micrographs of **a** bright field image MSP-2 sample, **b** dark field image of MSP-2 sample, **c** SAED pattern of MSP-2 sample

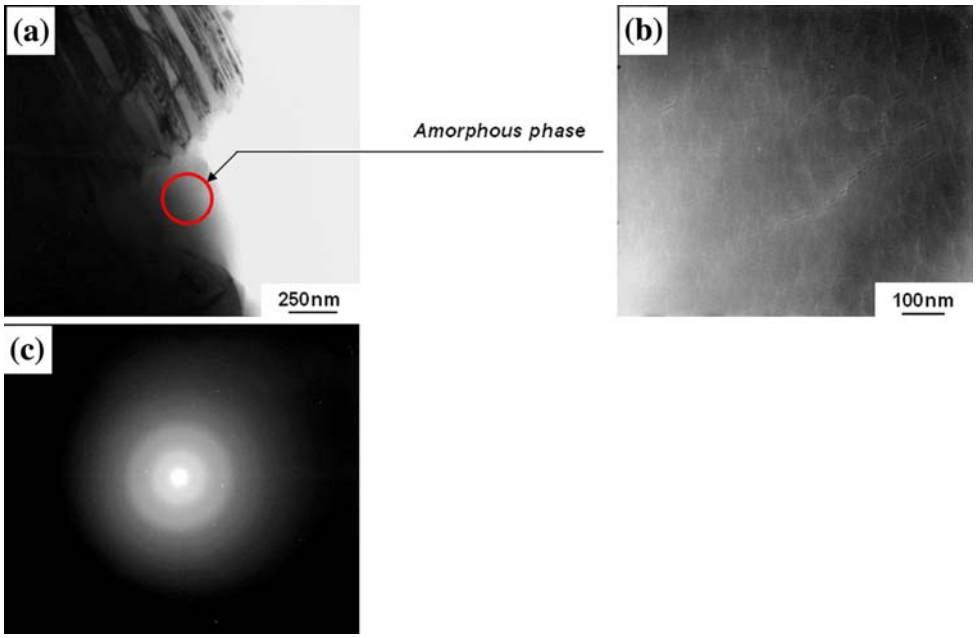

Fig. 7 TEM micrographs of **a** bright field image MSP-2 sample, **b** bright field image of MSP-2 sample, **c** SAED pattern of MSP-2 sample

taken from the marked region (circle) shows diffuse rings characteristic of an amorphous structure. In melt spinning there is a direct contact with a rotating copper wheel which quenches the molten material. The quenching rate depends on the molten metal temperature and wheel speed. In case of MSP-1 the lower wheel speed resulted in lower quenching

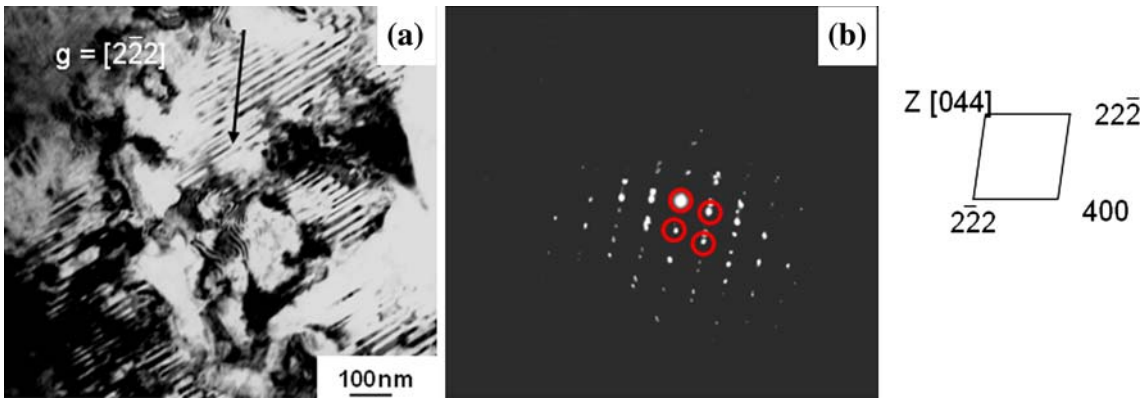

Fig. 8 TEM micrographs of **a** bright field image MSP-2 HT (annealed at 1000 °C/1 h) sample **b** SAED pattern of MSP-2 HT (annealed at 1000 °C/1 h) sample

rate and end up with fine crystals. In case of MSP-2 the higher wheel speed resulted in high quenching rate and which in turn resulted in martensite, nanoparticles of Ni_2MnGa, and amorphous phase at different locations of the ribbon. Local variations in under cooling from wheel side to free side could be the reason for formation of various phases as mentioned in different locations of the ribbon.

We have heat treated the MSP-1 and MSP-2 samples by annealing at 1000 °C/1 h and reported the analysis below.

Low wheel speed and high wheel speed ribbons annealed at 1000 °C/1 h (MSP-1 HT and MSP-2 HT)

X-ray diffraction of profile of MSP-1 HT sample (as shown in Fig. 1) confirms to austenite phase with $L2_1$ Huesler atomic order. No other reflections were observed as compared to MSP-1 sample. This confirms the absence of any amorphous content that could crystallize after annealing the sample at 1000 °C for 1 h.

Figure 8a, b shows the bright field TEM image and SAED pattern of MSP-2 HT sample. The bright field image (Fig. 8a) confirms to martensite phase with g-vector corresponds to [2 $\bar{2}$ 2] direction and SAED pattern (Fig. 8b) was taken by using [0 4 4] zone axis. The bright field image (Fig. 8a) clearly reveals very fine twins of martensite of about 20–25 nm size and the selected electron diffraction pattern (Fig. 8b) confirms the martensite phase belongs to non-modulated tetragonal structure. The XRD pattern of MSP-2HT (Fig. 1) confirms the existence of both martensite and gamma (γ) phases [21]. In the high speed ribbon, the amorphous and nanoparticles of Ni_2MnGa would transform to crystalline after annealing at 1000 °C. This could be confirmed by SAED pattern (Fig. 8c), which shows the spotty pattern as an indication of crystalline sample. Also the formation of gamma (γ) phase as confirmed from XRD results can be attributed to transformation of amorphous phase and nanoclusters of Ni_2MnGa, after annealing at 1000 °C.

Summary

Ni_2MnGa alloy upon rapid solidification by melt spinning at lower wheel speed (20 m/s) forms very fine micro crystals of austenite phase with average grain size about 80–180 nm. At higher wheel speed (30 m/s) it forms martensite phase with twins of 120°–125° included angle and average size about 20–120 nm and also consists of regions that contain uniformly distributed Ni_2MnGa nano particles of size 10–20 nm and an amorphous phase. The lower wheel speed (20 m/s) ribbon after annealing at 1000 °C for 1 h did not show any additional phases. However, the higher wheel speed (30 m/s) ribbon after annealing at 1000 °C for 1 h resulted in very fine martensite twins of size about 20–25 nm and (γ) gamma phase. Amorphous phase formation and crystallization upon heat treatment opens up further possibilities of metastable microstructures in Heusler alloys.

Acknowledgement We acknowledge Prof. K. Chattopadhyay of Indian Institute of Science for processing facilities.

References

1. Herlach DM (1994) Mater Sci Eng R 12:177
2. Smith CH (1993) In: H. Liebermann (ed) Rapidly solidified alloys: process, structure, properties and applications. Marcel Decker, New York, ISBN 0-8247-8951-2
3. Jones H et al (2001) Mater Sci Eng A 11–19:304
4. Ullakko K et al (1996) Appl Phys Lett 69:1966
5. Richard ML et al (2007) Phil Mag 87:3437
6. Ge Y (2007) The crystal and magnetic microstructure of Ni-Mn-Ga alloys. Doctoral thesis, ISBN 978-951-22-8661-4

7. Hakola A (2006) Thin-film deposition using laser ablation: application to ferromagnetic shape-memory materials and methods for spatial shaping of laser beams. Doctoral thesis, ISBN 951-22-8282-8
8. Prasad RVS, Phanikumar G (2009) Material Science forum: proceedings of the 5th international conference on solidification and gravity held at Miskolc-Lillafüred, Hungary (to be published)
9. Lanska N et al (1995) J Appl Phys 12:8074
10. Flemings MC (1974) Solidification processing. McGraw-Hill, New York
11. Rama Rao NV et al (2007) Scripta Mater 56:405
12. Niklasch D, Dadda J et al (2008) J Mater Sci 43:6890. doi:10.1007/s10853-008-2997-z
13. Gruner ME, Entel P, Opahle I et al (2008) J Mater Sci 43:3825. doi:10.1007/s10853-007-2291-5
14. Liu JY, Lu H, Chen JM et al (2008) J Mater Sci 43:4921. doi:10.1007/s10853-008-2716-9
15. Gialanella S, Ischia et al (2008) J Mater Sci 43:1701. doi:10.1007/s10853-007-2358-3
16. Gibson MA et al (1988) J Mater Sci 23:1164. doi:10.1007/BF01154574
17. Haddad-S M, Amberg G (1993) Int J Rapid Solidif 7:255–267
18. Liebermann HH (1979) IEEE Trans Mag 15(6):1393
19. Pons J et al (2000) Acta Mater 48:3027
20. Renhui W et al (2002) Acta Mater 50:1835
21. Ma Y et al (2007) Acta Mater 55:1533